Pharmacokinetic evaluation of [18F]PR04.MZ for PET/CT imaging and quantification of dopamine transporters in the human brain

Vasko Kramer, Carlos Juri, Patrick J. Riss, Rossana Pruzzo, Cristian Soza-Ried, Jonathan Flores, Ana Hurtado, Frank Rösch, et al.

European Journal of Nuclear Medicine and Molecular Imaging

ISSN 1619-7070

Eur J Nucl Med Mol Imaging
DOI 10.1007/s00259-019-04594-z

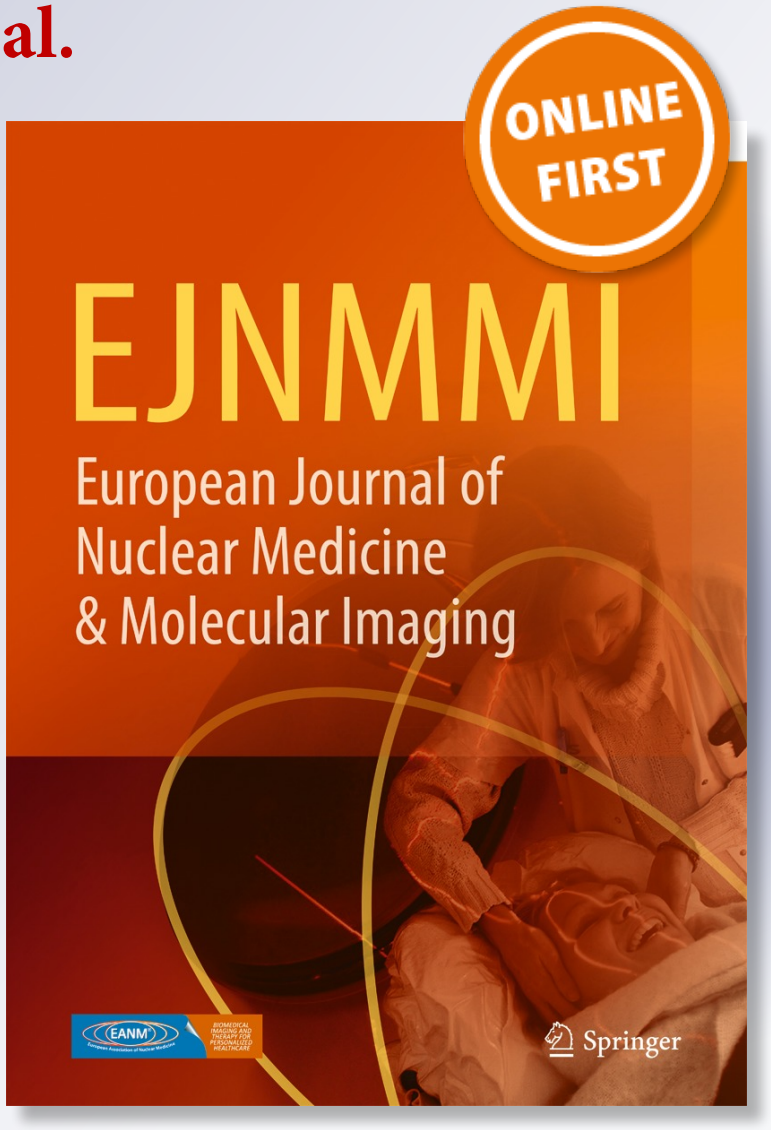

Springer

European Journal of Nuclear Medicine and Molecular Imaging
https://doi.org/10.1007/s00259-019-04594-z

ORIGINAL ARTICLE

Pharmacokinetic evaluation of [^{18}F]PR04.MZ for PET/CT imaging and quantification of dopamine transporters in the human brain

Vasko Kramer[1,2] · Carlos Juri[3,4] · Patrick J. Riss[5] · Rossana Pruzzo[1] · Cristian Soza-Ried[1] · Jonathan Flores[1] · Ana Hurtado[1] · Frank Rösch[6] · Pedro Chana-Cuevas[7,8] · Horacio Amaral[1,2]

Received: 8 July 2019 / Accepted: 23 October 2019

Abstract

Purpose Dopamine transporters (DAT) modulate pre-synaptic dopamine and physiological functions such as movement and reward. DAT also mirrors disease state in neurological disorders, rendering it an essential diagnostic target. [^{18}F]PR04.MZ is a new PET imaging agent for DAT with an improved affinity and selectivity profile, for which we here describe the complete pharmacokinetic evaluation in healthy controls.

Methods Thirty-two healthy subjects underwent T1-weighted MRI and dynamic PET scans for 180 min with arterial blood sampling (n = 5) or 90 min without blood sampling (n = 25) after injection of 197.6 ± 12.2 MBq [^{18}F]PR04.MZ. Blood and plasma metabolite analysis were performed. MRI-based normalization of brain images, delineation of VOIs, and kinetic modeling was conducted to determine distribution volumes (V_t) and binding potentials (BP_{nd}). The impact of scan duration was evaluated and repeated PET scans were performed to assess test-retest variability (n = 5). A static imaging protocol has been validated for clinical applications.

Results [^{18}F]PR04.MZ showed rapid metabolization in circulation, very high uptake in striatum and midbrain, and very low non-specific binding. The two-tissue compartment model 2TCM provided best fits for measured time-activity-curves and calculated V_ts in putamen, caudate, substantia nigra pars compacta (SNpc), and cerebellar cortex were 11.83, 9.73, 2.12, and 0.57, respectively. All non-invasive models correlated well with BP_{nd} values derived from 2TCM but underestimated DAT availability by about 28–33%. Of those, simplified reference tissue model (SRTM) provided the best fits, lowest Akaike Information Criteria values, and BP_{nd} values of 14.82, 11.95, and 2.63 in putamen, caudate, and SNpc, respectively. BP_{nd} estimates for striatal regions and SNpc were stable between 90 and 130 min post-injection. Test-retest results were excellent, showing low variability in all and excellent reliability in most relevant regions. Static imaging from 60 to 90-min post-injection is a viable alternative for quantification.

Conclusions [^{18}F]PR04.MZ is a PET tracer with very high affinity, selectivity, and specific uptake in striatum and midbrain. 2TCM and SRTM provide good fits, high and stable V_ts or BP_{nd}s, and good test-retest reliability for precise quantification of DAT in human subjects.

Keywords [^{18}F]PR04.MZ · Pharmacokinetics · Dopamine transporter · Parkinson's disease · PET/CT

Introduction

The neurotransmitter dopamine mediates physiological functions such as movement, cognition, mood, and reward. Extracellular dopamine concentration is modulated by the dopamine transporter (DAT), a plasma membrane protein that facilitates presynaptic reuptake [1]. The DAT is also involved in neurotoxicity and mirrors disease state, including movement disorders, attention deficit hyperactivity disorder (ADHD), and drug abuse, rendering it an important diagnostic target [2]. Particularly in Parkinson's disease (PD),

This article is part of the Topical Collection on Translational research

Electronic supplementary material The online version of this article (https://doi.org/10.1007/s00259-019-04594-z) contains supplementary material, which is available to authorized users.

✉ Vasko Kramer
vkramer@positronpharma.cl

Extended author information available on the last page of the article

Published online: 01 December 2019

characterized by pathological aggregation of miss-folded α-Synuclein and the formation of Lewy-bodies, leading to degeneration of dopaminergic, nigro-striatal neurons, DAT is an excellent biomarker for diagnostic imaging [3, 4].

One clinical application is the differential diagnosis between idiopathic PD and essential tremor for which the FDA-approved single-photon emission computed tomography tracer Datscan™ (Ioflupane I-123) is the standard of care. Although positron emission tomography (PET) is the superior imaging technique, no PET tracer has been approved for the same purpose to date which might relate to higher costs and complicated quantification of earlier generations of DAT tracers. Nevertheless, at sites where Datscan™ has not been approved or is not available or when precise quantification for clinical research is necessary, DAT PET imaging is a viable alternative. Different radiopharmaceuticals have been translated into clinical testing for this purpose such as [^{18}F]FP-CIT, [^{18}F]FE-CNT, [^{18}F]FE-PE2I, [^{18}F]LBT-999, and others [5–11]. Still, there is still an unmet need for a clinically validated, high-affinity, selective PET radiotracer suitable for accurate quantification of DAT, especially in the substantia nigra pars compacta (SNpc) where nigrostriatal neurons originate.

The tropane derivative PR04.MZ is a high-affinity (IC_{50}hDAT 3.3 nM), DAT-selective (SERT/DAT-selectivity > 74; NET/DAT-selectivity > 10), competitive inhibitor of monoamine reuptake [12, 13]. Its binding profile exceeds the figures reported for most of the established DAT-ligands, providing a superior selectivity [14–16]. A robust labeling procedure has been described and [^{18}F]PR04.MZ showed very high uptake in striatal and midbrain regions and low non-specific binding in PET imaging studies in both, healthy Wistar rats and non-human primates [13, 17, 18]. Furthermore, [^{18}F]PR04.MZ exhibited fast tracer kinetics allowing for quantification within a reasonable time frame. Binding in striatal regions was completely displaceable with β-CFT (WIN 35,428) in autoradiography on rat brain slices [13, 18].

The promising pre-clinical data and potential for clinical translation were confirmed by the excellent imaging properties of [^{18}F]PR04.MZ in a recent case study of Holmes Tremor published by our group [19]. We further reported on the clinical potential of this new PET tracer for the detection of nigrostriatal degeneration in patients under evaluation for movement disorders [20, 21]. We are interested in DAT imaging in patients who are at risk of developing PD, particularly those with REM sleep behavior disorder or DiGeorge-Syndrome, where precise quantification is crucial. We, therefore, present here the pharmacokinetic validation of [^{18}F]PR04.MZ in healthy human subjects including metabolism, regional brain uptake, kinetic modeling, impact of scan duration, and test-retest variability.

Materials and methods

Radiochemistry

[^{18}F]PR04.MZ was produced under GMP-compliant conditions using a modified procedure similar to those previously described [13] and as detailed in the supplemental information (SI). Briefly, [^{18}F]PR04.MZ was obtained as a sterile solution after 53 min in 27.6 ± 5.5% radiochemical yield (n.d.c.), > 98% radiochemical purity, and specific activities of 121 ± 54 GBq/μmol.

Subjects

Thirty-two healthy controls (HC) (age 55.5 ± 18.2 years, 22 males) were included in the study, which was approved by the regional ethics committee board (CEC-SSM-Oriente, permit 20140520), and written informed consent has been obtained from all participants. Inclusion criteria were the age of 20–80 years and showing no signs of neurological or psychiatric disorders as confirmed by standard neurological examination. Exclusion criteria were smoking and use of psychoactive substances. Subjects fasted for at least 12 h before tracer injection, including caffeine restriction. For detailed subject demographics see SI.

PET imaging

A cross-calibration of all devices (PET scanner, dose calibrator, well counter, and automated blood sampler) was performed on each day using an internal standard. The mean ± SD of the administered mass of [^{18}F/^{19}F]PR04.MZ was 1.58 ± 1.31 μg (range, 0.1–4.7 μg) and the mean administered activity was 197.6 ± 12.2 MBq (range, 181.3–227.2 MBq). There were no adverse or clinically detectable pharmacologic effects in any of the 32 subjects and no significant changes in vital signs were observed. For all participants, a low-dose CT scan was performed for attenuation correction. Simultaneously with tracer injection, a dynamic PET scan (Siemens mCT Flow, Erlangen, Germany) was performed in LIST-Mode for 180 min with arterial blood sampling (n = 5) or 90 min without blood sampling (n = 27) and head movement was minimized using a head immobilization system. 2/5 subjects were not able to undergo complete imaging procedure, and scans were aborted at t = 85 and 130 min post-injection (p.i.). Furthermore, 5/32 HCs participated in a second PET scan with the tracer, 14 days after baseline PET to evaluate test-retest variability.

Input function measurement

Radioactivity in whole blood (WB) was continuously measured for up to 120 min using an automated blood sampler

(Twilite 2, Swisstrace), synchronized to the PET camera, for n = 4 subjects. For 1/5 subjects, no useful input function could be obtained due to blood clotting. The flow rate was changed stepwise from 5 mL/min (6 min) to 2.5 mL/min (5 min) to 0.33 mL/min (109 min). Arterial blood samples for metabolite analysis (10 mL) were drawn manually at 5, 10, 20, 40, 60, 90, and 120 min p.i. The activity values obtained at each timepoint were corrected for decay to the time of injection.

Radiometabolite analysis

For n = 5 subjects, whole blood samples (2 × 4.5 mL) were centrifuged (4000 rpm, 5 min) and radioactivity in WB and plasma was measured using a well counter to calculate plasma/WB ratios. A total of 1.5 mL of the plasma fraction was added to 3.0 mL acetonitrile followed by centrifugation (4000 rpm, 5 min) to remove protein precipitates. A volume of 2 mL of the supernatant plasma was filtered (0.45 μM, Whatman GD/X) and injected into an analytical HPLC system (see SI).

Magnetic resonance imaging acquisition

All subjects were scanned in a 1.5 T magnetic resonance imaging (MRI) scanner from Gyroscan Intera, Phillips Medical System, Best, the Netherlands. 3D T1-weighted MR images (isotropic 1 × 1 × 1 mm resolution) were acquired using the following parameters: T1 protocol; repetition time = 7.3 ms; echo delay time 3.3 ms; inversion time = 815 ms, and flip angle = 8°.

Image post-processing and analyses

PET images were corrected for scattering, attenuation, and TOF and reconstructed by an iterative algorithm (2 iterations and 21 subsets) followed by post-reconstruction smoothing (Gaussian, 4 mm FWHM). The 90-min dynamic PET scans were reframed into 38 static frames (6 × 10 s, 6 × 20 s, 7 × 60 s, 5 × 120 s, 14 × 300 s) and the 180 min PET scans were reframed into 61 static frames (10 × 6 s, 6 × 20 s, 6 × 60 s, 8 × 120 s, and 31 × 300 s). Images consisted of 110 planes of 256 × 256 voxels of 1.59 × 1.59 × 1.5 mm^3. PET images were visually inspected and corrected for motion. Volumes of interest (VOI) were generated from a three-dimensional maximum probability atlas [22] after MRI-based co-registration and normalization (PNeuro V3.6, PMod Technologies). Time-activity curves (TACs) were generated for relevant brain VOIs (anterior, posterior and total putamen, caudate nucleus, nucleus accumbens, substantia nigra pars compacta (SNpc), thalamus, neocortex, and cerebellum—all divided into left, right, and total). Standardized uptake values (SUVs) were obtained by normalizing radioactive concentrations in VOIs to the injected dose per body weight. For the evaluation of static imaging protocols, frames from 60–90 and 75–90 min p.i. were averaged and the same VOIs were applied.

Quantification of [^{18}F]PR04.MZ binding

Kinetic modeling was performed (PKin V3.4, PMOD Technologies) using radioactivity concentrations of the parent compound in plasma as reference for fitting of tissue TACs. Distribution volumes (V_ts) were derived from one- and two-tissue compartment models (1TCM and 2TCM) fitting three (K1, k2, VB) or five parameters (K1, k2, k3, k4, VB), respectively and using Logan plot graphical analyses (Logan). The non-displaceable binding potentials (BP_{nd}) for the 2TCM were derived from 2-TCM-V_ts as follows: BP_{nd} = V_t (target)/V_t (cerebellum)-1. For non-invasive models, BP_{nd} values were calculated using Logan non-invasive graphical analysis (NIGA), multi-linear reference tissue model (MRTM0) and simplified reference tissue model (SRTM). The cerebellar cortex was used as reference tissue for all BP_{nd} models. All applied kinetic models were described in detail by Lammertsma et al. [23, 24]. Goodness-of-fit was evaluated using the Akaike Information Criterion (AIC). For static image quantification, specific binding ratios (SBR), defined by SBR = (SUV (region)–SUV (cerebellum))/SUV (cerebellum), were calculated for VOIs outlined on averaged images from 60–90 and 75–90 min p.i.

Stability of outcome measures

To investigate the effect of the scan duration on BP_{nd} values and to determine optimal time points for stable outcome measures, tissue TACs were truncated in 10-min increments (from 180 to 30 min) for n = 3 subjects. The truncated TACs were used to derive BP_{nd} values using SRTM for each region and subject. For each truncation, BP_{nd} values were expressed as the percentage of peak BP_{nd} reached during the scan and averaged as mean ± SD.

For future clinical applications, the optimal time points for static imaging and the effect of the scan duration on quantification were evaluated. Therefore, specific binding ratios (SBR) and relative SBRs (normalized to maximum SBR reached) were calculated for each time frame from 0 to180 min and compared to quantitative BP_{nd} values for n = 3 subjects.

Test-retest variability

The test-retest variability (VAR) was evaluated by comparing BP_{nd} values, derived from SRTM, from baseline and follow-up PET scans for n = 5 subjects, performed under the same conditions. Both scans were performed exactly 14 days apart and injected dose and mass did not differ significantly. VAR

and interclass correlation coefficient (ICC) as a measure of reliability were calculated as previously described [25]. Briefly, VAR was calculated as mean ± SD of the individual variability defined as the absolute value of the difference between the test and retest values, divided by the mean of both values. The ICC was calculated according to the following equation and as detailed in supplemental information: ICC = (BSMSS-WSMSS)/(BSMSS+WSMSS). VAR of 10–20% and 0–10% were considered as moderately good and very good, respectively. ICC values of < 0.7, 0.7–0.79, 0.8–0.89, and 0.9–1.0 indicate poor, acceptable, good, and excellent reliability, respectively. The same evaluations of VAR and ICC values were carried out for SBR values derived from static images.

Statistical analysis

For comparison of V_t and BP_{nd} between models, we used the Kruskal-Wallis and the Dunn Multiple Comparison as a post hoc non-parametric test. Shapiro-Wilk test and Q-Q plots were used to check for normal distribution of the data. To analyze differences between models regarding AIC criteria, we used two-tailed unpaired Student's *t* test. To assess the equality of variances between groups, the Levene's test was used. In all the comparisons, the results were considered significant when *p* values were less than 0.05. All the comparison analysis was performed using the STATA software, version 14.

Results

Metabolism and arterial input function

The plasma-to-WB ratio, HPLC metabolite analysis, metabolite and parent ratio in plasma, decay-corrected activity in WB, and corrected parent input function in plasma are shown in Fig. 1. A peak activity concentration of 28.2 kBq/mL was reached after 35–40 s p.i. in WB. The activity distribution ratio between WB and plasma was stable at 1.31 during the sampling window from 0–120 min p.i (n = 5 subjects). Besides the unchanged parent compound (R_t = 8.8 min), we found one polar metabolite eluting with the solvent front from HPLC after 2.0 min (see Fig. 1a). [^{18}F]PR04.MZ is metabolized very fast with a biological half-life of approximately 11–12 min during the initial period of the scan. The averaged, corrected arterial input function (AIF, parent concentration in plasma) for n = 3 subjects is shown in Fig. 1e. Peak uptake of 24.4 kBq/mL was reached after 35–40 s p.i., decreasing rapidly to 10.0 kBq/mL at 3 min p.i. and 1.8 kBq/mL at the end of sampling.

[^{18}F]PR04.MZ distribution in the human brain

[^{18}F]PR04.MZ showed very high uptake in DAT-rich striatal regions, high uptake in the midbrain region known to express DAT, and very low non-specific binding in other brain regions such as the cerebellum, cortical areas, and white matter (see Fig. 2a). [^{18}F]PR04.MZ readily entered the brain. Distribution in DAT-rich brain regions reached peak SUV values of 10.8 ± 3.2 after 37 min in putamen, 8.6 ± 2.2 after 43 min in caudate nucleus and 6.0 ± 1.2 after 7 min in SNpc followed by slow washout until the end of the scan (see Fig. 2b). The rate of uptake and washout follows the expected pattern of DAT distribution (putamen > caudate > SNpc). SUV values in regions with negligible DAT expression, such as cortical cerebellar cortex, reached peak uptake of 5.0 ± 1.2 at 2 min p.i. and showed fast clearance reaching very low nonspecific uptake with SUV values below 0.48 ± 0.10 at 80 min p.i.

Also, low but detectable retention was observed in the thalamus when compared to the cerebellar cortex during the first 60 min p.i. with peak SUV values of 5.7 ± 1.2 at 3 min p.i. followed by fast washout reaching cerebellar concentrations at around 100 min p.i. This significant uptake was more pronounced in subthalamic and central regions of the thalamus and was not observed in other cortical or subcortical areas.

Quantification and kinetic modeling of [^{18}F]PR04.MZ binding

V_ts and BP_{nd}s for [^{18}F]PR04.MZ at 130 min p.i. were calculated using different invasive and non-invasive models, TACs were visually inspected for the goodness of fit and AIC values were compared (for n = 3 subjects). The fits for the 2TCM correlated very well with the measured tracer distribution over time in DAT-rich brain regions and V_t values in the putamen, caudate, SNpc, and cerebellar cortex were 11.83, 9.73, 2.12, and 0.57, respectively. 1TCM resulted in poorer fits, overestimating tracer distribution in initial time frames while underestimating distribution in later time frames when compared to measured data (see SI). This is also reflected by lower AIC values, indicating better fits, for the 2TCM versus 1TCM in the putamen and caudate ($p < 0.001$) and SNpc ($p < 0.05$) when comparing AIC criteria for the goodness of fit. Quantification with 1TCM resulted in an underestimation of V_t of 38% when compared to 2TCM for all brain regions ($p < 0.001$). Logan graphical analysis resulted in similar, but slightly lower, V_ts when compared to 2TCM. Within the invasive models, 2TCM provided the best fits and estimates for V_t (see Table 1 and Fig. 3). To compare non-invasive reference models with invasive models, BP_{nd} values were calculated for the 2TCM and compared to BP_{nd} values derived from SRTM, MRTM0, and NIGA. All tested reference tissue models correlated well with 2TCM but resulted in an underestimation of BP_{nd} values of 28–33% in high-density regions

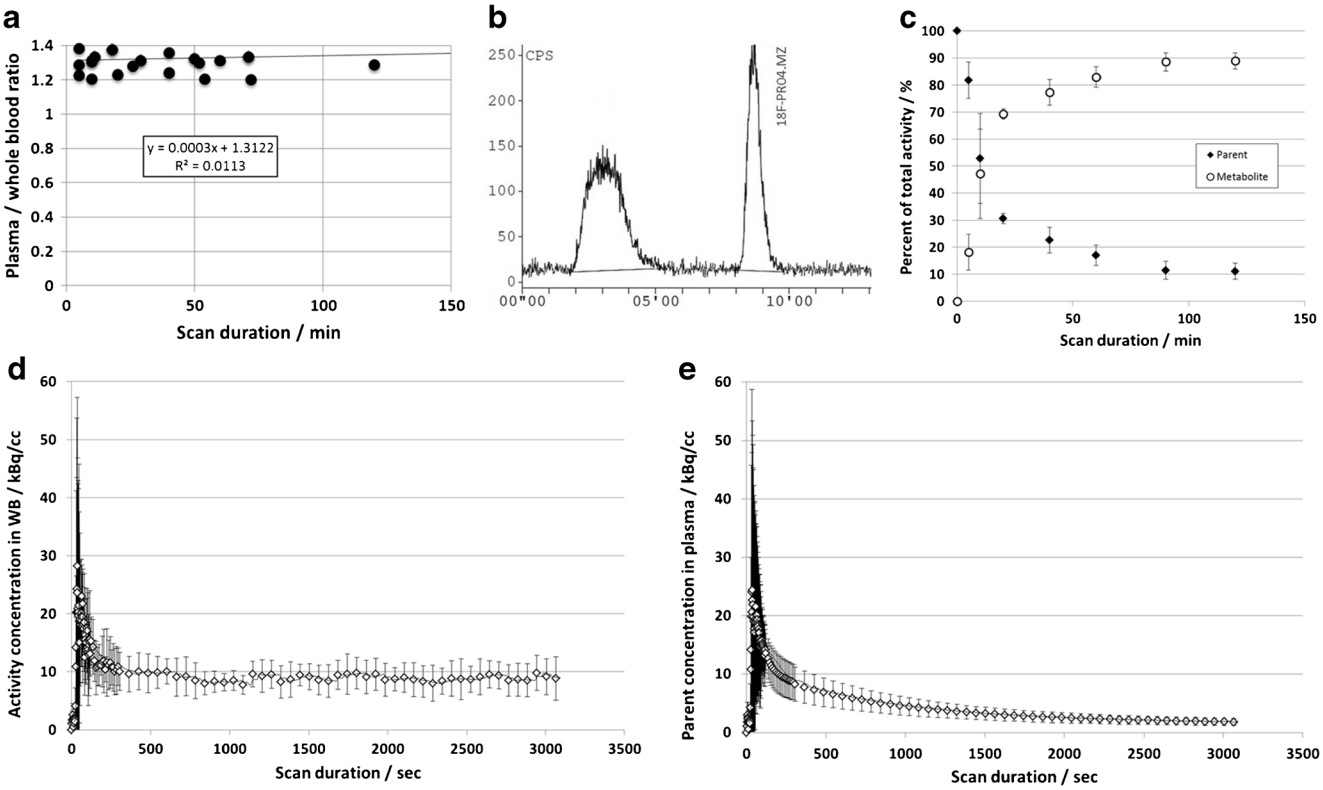

Fig. 1 **a** Activity distribution ratio between WB and plasma from $n = 5$ subjects. **b** HPLC metabolite analysis of [^{18}F]PR04.MZ, polar metabolite at $t = 2.0$ min, parent compound at $t = 8.2$ min. **c** Parent and metabolite fractions in plasma (mean ± SD, $n = 5$ subjects). **d** Decay-corrected activity concentration in WB. **e** Corrected arterial input function in plasma, (**d** and **e**: mean ± SD, $n = 3$)

of DAT ($p < 0.05$) which was not significant in SNpc ($p > 0.05$). For comparison of different reference models with each other, a total of $n = 30$ subjects were included. BP_{nd} values for SRTM were slightly lower than for MRTM0 and NIGA although not statistically significant. SRTM provided better fits in all brain regions than MRTM0 when comparing AIC values

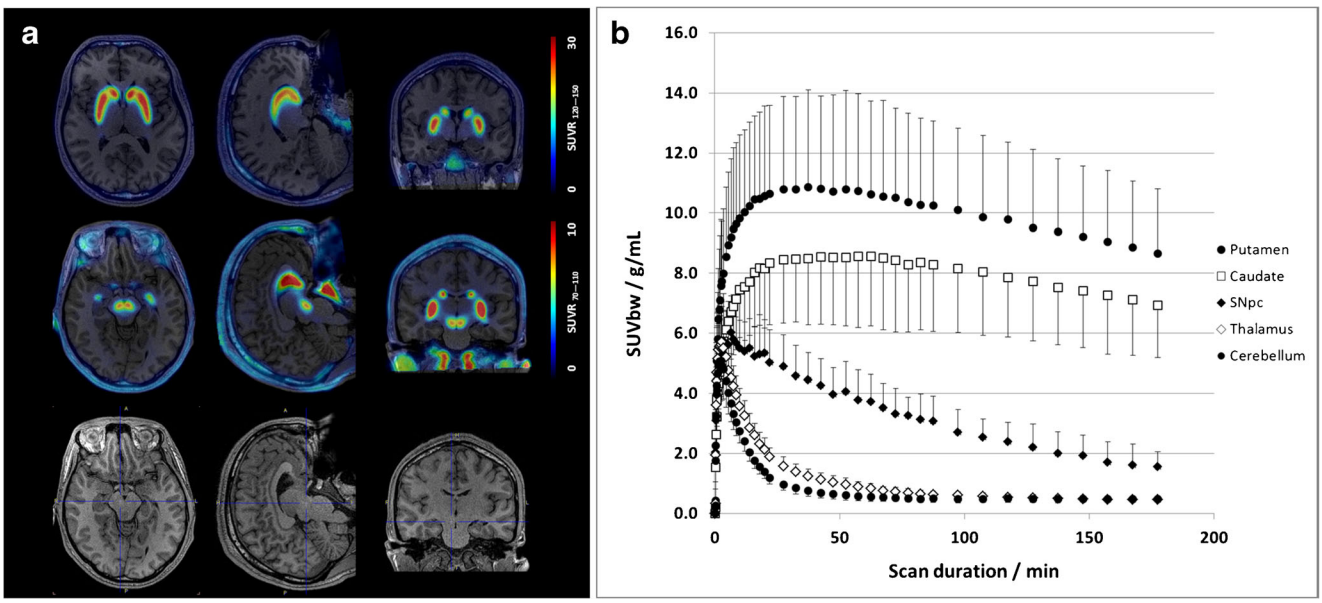

Fig. 2 **a** Averaged PET/MRI fusion images of [^{18}F]PR04.MZ, transversal, sagittal, and coronal images (from left to right), averaged frames 120–150 min p.i. (upper row) and 70–100 min (middle row). Images are scaled to SUV ratio ($SUVR = SUV_{region}/SUV_{cerebellum}$). Lower row: corresponding MRIs; **b** Averaged TACs (mean ± SD; $n = 3$) for [^{18}F]PR04.MZ in putamen, caudate nucleus, SNpc, thalamus, and cerebellum

($p < 0.001$). Therefore, SRTM provides the best estimates for [^{18}F]PR04.MZ BP_{nd} values within the non-invasive reference models.

Stability of outcome measures

To investigate the effect of the scan duration, BP_{nd} values for each truncated curve were calculated as described (see Fig. 4a, b). By analyzing scan durations between 45 and 180 min, we found maximum BP_{nd} values at 90 min p.i. for SNpc, 130 min p.i. for caudate and 150 min p.i. for putamen, which is in accordance with expected DAT concentrations in those regions (putamen > caudate > SNpc). When considering a variation of less than 5% of maximum BP_{nd} as stable quantification outcome, the optimal scan duration for quantification is > 50 min for SNpc and > 90 min for caudate and putamen.

In order to evaluate a simplified, static imaging protocol for future studies and applications in clinical management of movement disorders, we compared SBRs with BP_{nd} values derived from SRTM. Figure 4 shows BP_{nd} values, relative BP_{nd} values, total SBRs, and relative SBRs at different scan durations for up to 180 min. In contrast to quantification with kinetic modeling, we found maximum SBR values at 50–70 min p.i. for SNpc and at 80–100 min p.i. for caudate nucleus and putamen. While BP_{nd} values for SNpc were stable from 50–130 min p.i., SBR showed rapid decline after 90 min p.i. Nevertheless, SBR from averaged frames between 60–90 min and 75–90 min p.i. were within 94% and 92% of maximum SBR, respectively.

Figure 5 shows graphical fits for correlations between BP_{nd} values at 90 min p.i., SBR values from averaged 60–90 min frames, and from 75–90 min frames for SNpc, caudate and putamen (n = 20 HCs). At both time intervals, SBRs showed

Table 1 V_ts and BP_{nd}s of [^{18}F]PR04.MZ at 130 min p.i., obtained by model calculations using 2TCM, 1TCM, and Logan graphical analysis with AIF, and NIGA, MRTM0, and SRTM with cerebellar cortex as reference region, respectively. Values are expressed as mean ± SD from n = 3 subjects

	Invasive models			Non-invasive reference models			
Region	2TCM V_t (mL/cm^3)	1TCM V_t (mL/cm^3)	Logan V_t (mL/cm^3)	2TMC BP_{nd} (unitless)	NIGA BP_{nd} (unitless)	MRTM0 BP_{nd} (unitless)	SRTM BP_{nd} (unitless)
Putamen_r	11.81 ± 1.77	7.87 ± 0.71	11.22 ± 0.76	19.74 ± 3.97	15.31 ± 2.77	15.22 ± 2.78	14.93 ± 2.75
Putamen_t_ant	11.97 ± 1.68	8.10 ± 0.75	11.35 ± 0.97	20.03 ± 3.89	15.80 ± 2.99	15.63 ± 3.04	15.41 ± 2.98
Putamen_r_post	11.46 ± 2.19	7.49 ± 0.74	11.29 ± 0.61	19.13 ±4.59	14.43 ± 2.46	14.14 ± 2.06	14.17 ± 2.46
Putamen_l	11.99 ± 2.14	7.77 ± 0.53	11.60 ± 1.01	20.07 ± 4.61	15.28 ± 2.69	15.50 ± 3.02	14.71 ± 2.38
Putamen_l_ant	11.94 ± 2.18	7.90 ± 0.59	11.65 ± 1.09	19.99 ± 4.72	15.53 ± 2.76	15.59 ± 2.95	14.91 ± 2.51
Putamen_l_post	11.85 ± 2.32	7.62 ± 0.49	11.56 ± 0.94	19.83 ± 4.89	15.03 ± 2.62	15.04 ± 2.75	14.45 ± 2.26
CaudateNucl_l	9.93 ± 1.65	6.56 ± 0.66	9.61 ± 0.46	16.44 ± 3.63	12.53 ± 2.33	12.50 ± 2.16	11.95 ± 2.01
CaudateNucl_r	9.56 ± 2.00	6.54 ± 0.69	9.38 ± 0.77	15.81 ± 4.16	12.45 ± 2.51	12.39 ± 2.54	11.96 ± 2.22
NuclAccumb_l	7.75 ± 1.83	5.19 ± 0.73	6.76 ± 1.25	12.66 ± 3.82	9.56 ± 2.58	9.82 ± 2.48	9.77 ± 2.48
NuclAccumb_r	6.55 ± 2.01	4.35 ± 1.25	5.34 ± 1.71	10.50 ± 3.88	7.68 ± 2.87	7.93 ± 2.49	8.37 ± 3.20
Thalamus_l	0.65 ± NA*	0.68 ± 0.07	0.85 ± 0.08	0.16 ± NA*	0.42 ± 0.09	0.44 ± 0.07	0.43 ± 0.08
Thalamus_r	0.70 ± NA*	0.67 ± 0.08	0.81 ± 0.07	0.24 ± NA*	0.35 ± 0.13	0.39 ± 0.10	0.37 ± 0.11
SN_{pc}_l	2.07 ± 0.26	1.40 ± 0.34	2.18 ± 0.29	2.64 ± 0.57	2.56 ± 0.58	2.74 ± 0.68	2.66 ± 0.61
SN_{pc}_r	2.05 ± 0.40	1.36 ± 0.25	2.11 ± 0.32	2.59 ± 0.77	2.45 ± 0.56	2.82 ± 0.93	2.60 ± 0.58
Neocortex	0.52 ± 0.07	0.55 ± 0.10	0.65 ± 0.11	-0.09 ± 0.09	0.05 ± 0.04	0.05 ± 0.04	0.00 ± 0.0†
Putamen	11.83 ± 1.97	7.82 ± 0.62	11.44 ± 0.93	19.79 ± 4.34	15.33 ± 2.77	15.32 ± 2.77	14.82 ± 2.56
Putamen_ant	12.00 ± 1.82	8.02 ± 0.65	11.49 ± 1.14	20.09 ± 4.11	15.70 ± 2.93	15.68 ± 2.95	15.17 ± 2.75
Putamen_post	11.60 ± 2.29	7.53 ± 0.62	11.37 ± 0.72	19.39 ± 4.82	14.87 ± 2.60	14.87 ± 2.68	14.32 ± 2.34
CaudateNucl	9.73 ± 1.83	6.55 ± 0.67	9.48 ± 0.68	16.11 ± 3.92	12.51 ± 2.40	12.51 ± 2.45	11.95 ± 2.11
NuclAccumb	6.96 ± 1.79	4.84 ± 0.90	6.52 ± 1.16	11.27 ± 3.67	9.15 ± 2.65	8.90 ± 2.33	9.15 ± 2.70
Thalamus	0.67 ± NA*	0.67 ± 0.05	0.83 ± 0.07	0.20 ± NA*	0.38 ± 0.11	0.41 ± 0.08	0.40 ± 0.09
SN_{pc}	2.12 ± 0.35	1.41 ± 0.31	2.16 ± 0.31	2.71 ± 0.68	2.51 ± 0.57	2.73 ± 0.71	2.63 ± 0.59
Cereb_cortex	0.57 ± 0.03	0.57 ± 0.03	0.65 ± 0.08	NA			

Vt, distribution volume; *BPnd*, non-displaceble binding potential; *NA*, does not apply; *ant*, anterior; *post*, posterior; SN_{pc}, substantia nigra pars compacta; *l*, left; *r*, right

*Model calculations for 2TCM failed in Thalamus in n = 2 subjects

†Model calculations for SRTM in neocortex failed in n = 1 subject

good correlation with BPnd values but a positive bias of approximately 50%. Correlation between SBR after 60–90 and 75–90 min p.i. was excellent and results were almost identical.

Test-retest variability

To evaluate the test-retest variability we compared both VAR and ICC between baseline and follow-up PET scans for $n = 5$ subjects. The thalamus and neocortical regions were excluded from the analysis due to very low specific binding in these regions. VAR between test and retest was very good (< 10%) in all brain regions. The highest variability between scans was found in right posterior putamen (9.4 ± 5.9%), left posterior putamen (7.7 ± 3.2%), and total posterior putamen (6.2 ± 3.2%) followed by nucleus accumbens. Reliability between test and retest was found to be poor in left SNpc (0.47), acceptable in right SNpc (0.79), good in right posterior putamen (0.80), posterior putamen (0.88), and SNpc (0.80), and very good (0.9–1.0) in all other regions, as indicated in Table 2. In comparison to quantitative modeling data, VAR and reliability of SBR from static images were slightly lower but still very good. Only for nucleus accumbens VAR was only moderately good (11.1–13.0%).

Discussion

The present study was focused on the pharmacokinetic evaluation of [^{18}F]PR04.MZ in the brain of healthy human subjects.

Upon injection, [^{18}F]PR04.MZ was metabolized quickly with a plasma half-life of approximately 11.5 min. Besides the parent compound, we found one polar metabolite eluting after 2.0 min from the HPLC and no lipophilic metabolites likely to cross the blood-brain barrier and interfere with the methods used for quantification. The polar metabolite was retained quantitatively on a strong anion exchange cartridge and whole-body images showed some retention in bone (see SI). This implicates that the only metabolite found in plasma corresponds to free ^{18}F-fluoride ion.

In the brain, [^{18}F]PR04.MZ showed very high uptake in striatal regions and SNpc, following the expected pattern of DAT distribution (putamen > caudate > SNpc), and negligible non-specific binding in other regions of the brain. Despite the slow washout in high-density regions and low dissociation constants k_4, stable region-to-cerebellum ratios and transient equilibrium were reached within 90 min. This might be due to the relatively fast metabolism and elimination of the parent compound from the plasma compartment. The high region-

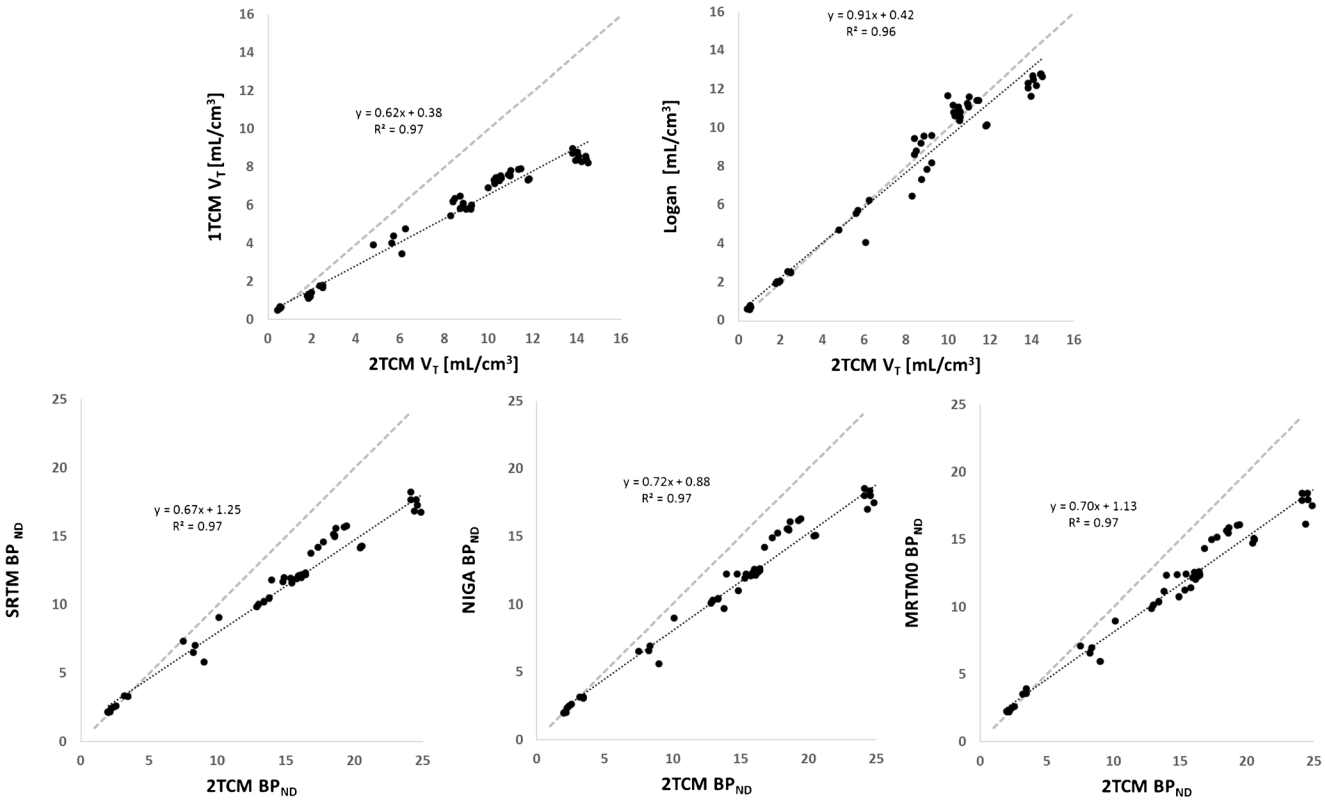

Fig. 3 **a**, **b** Linear regression analyses for the correlation between V_ts of invasive models and **c**–**e** BP_{nd} values of non-invasive models versus BP_{nd} derived from 2TCM. Correlation analysis for V_t included a total of 69 regions from $n = 3$ subjects as shown in Table 1. Correlation analysis for BP_{nd} values included a total of 54 regions from $n = 3$ subjects. Black dotted lines show linear regression. The regression equation for each correlation is displayed in each plot. Gray dotted lines represent line of identity

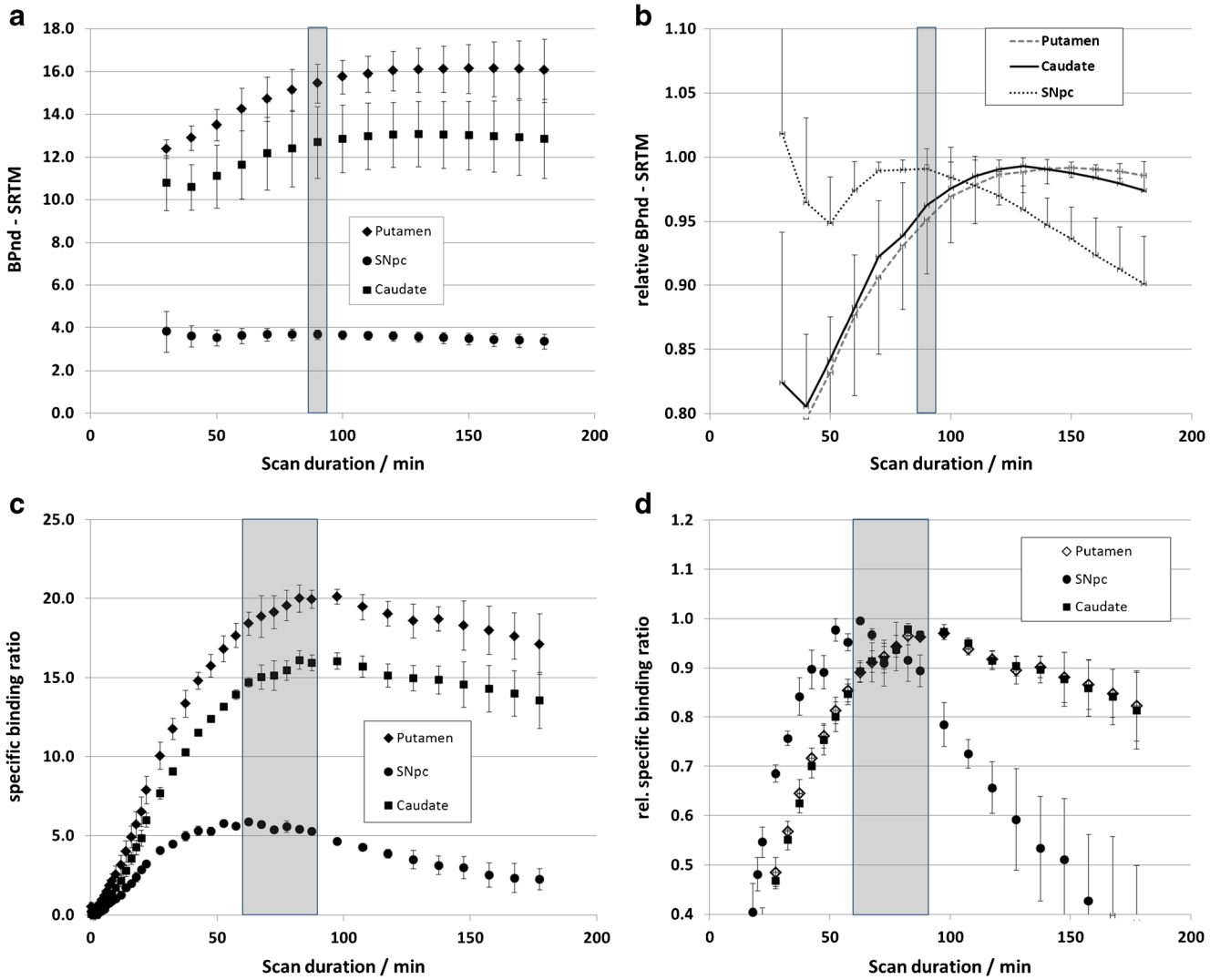

Fig. 4 **a** BP_{nd} values vs. scan duration for SNpc, caudate, and putamen. **b** Relative BP_{nd} values as a percentage of peak BP_{nd} vs. scan duration for SNpc, caudate, and putamen. **c** SBR values vs. scan duration for SNpc, caudate and putamen. **d** Relative SBR values vs. scan duration for SNpc, caudate, and putamen; all data presented as mean ± SD, $n = 3$)

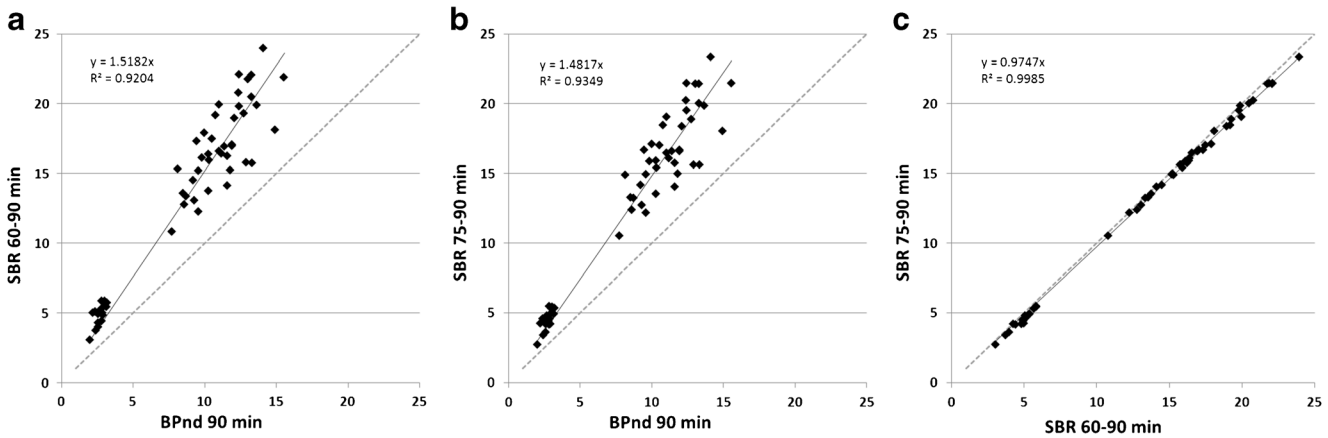

Fig. 5 Linear regression analyses for the correlation between **a** BPnd 90 min p.i. and SBR from 60–90 min p.i., **b** BPnd 90 min p.i. and SBR from 75–90 min p.i., and **c** SBR 60–90 min p.i. and from 75–90 min p.i. Correlation analysis included a total of 60 regions (SNpc, caudate, and putamen) from $n = 20$ subjects. Black dotted lines show linear regression. The regression equation for each correlation is displayed in each plot. Gray dotted lines represent line of identity.

to-cerebellum uptake ratios provide an excellent imaging contrast, reflecting the high affinity (IC_{50} = 3.3 nM) and selectivity measured in vitro [12].

In order to evaluate a reliable method for DAT quantification, we compared different invasive and non-invasive models, often used for brain receptor quantification. Of the invasive models, the 2TCM provided the highest V_ts, best fits of the experimental data, and lower AIC values when compared to 1TCM and Logan graphical analysis. Quantification with the 1TCM resulted in a significant underestimation of V_t, when compared to 2TCM and Logan. This can be explained by initial overestimation and later underestimation of local tracer distribution when comparing the 1TCM curve fit to the experimental TAC (see SI), resulting in smaller areas under the curve and thus lower V_ts for this model.

Since the acquisition of the arterial input function is impractical for routine application, experimentally challenging and uncomfortable, we evaluated the reference models SRTM, MRTM0 and NIGA for non-invasive quantification. All reference models correlated very well (R^2 = 0.97) with BP_{nd} values derived from the invasive 2TCM but resulted in an underestimation of 28–32% ($p < 0.05$). Similar underestimations have also been observed for other DAT PET tracers and receptor ligands, which might be an intrinsic limitation of the SRTM model, due to violations of the assumptions made therein [6]. However, since the correlation with the 2TCM is excellent and stable across all brain regions, the induced bias can be predicted and should not have an impact on comparative studies. Within the reference models, the SRTM provided the best fits and lowest AIC values. This is in line with published results for the kinetics of other DAT ligands, which can be best described and quantified using 2TCM and SRTM [5–7, 9].

Very high BP_{nd} values were observed in DAT rich regions, including SNpc where precise quantification of DAT is challenging. Since the reported in vitro selectivity of [^{18}F]PR04.MZ for DAT over SERT is over 74-fold, we can assume that this signal measured in SNpc is specific for DAT. This, in particular, is a significant advantage of this new tracer and might have a clinical impact for patients being evaluated for movement disorders in the future.

We studied the impact of scan duration on measurement outcomes and found that stable BP_{nd}s (< 5% deviation from BP_{nd} max.) can be obtained between 50 and 130 min p.i. for SNpc and after 90 min p.i. for caudate and putamen. This difference was expected and can be explained by the known DAT availability in those regions where transient equilibrium is reached earlier for lower DAT concentrations in SNpc. Nevertheless, the time-dependent variation of BP_{nd} is rather low and stable results can be derived within 90 min p.i.

For applications in clinical routine, non-invasive, static imaging protocols and simplified quantification methods are desired. We therefore compared SBR to BP_{nd} values derived from SRTM at different time frames during the 180 min scan

Table 2 Baseline and Retest BP_{nd} values (mean ± SD), total BP_{nd} values, between subjects SD and %CV, within subjects SD and %CV, VAR and ICC values for analyzed regions

Region	BPnd Baseline		BPnd Retest		Mean BPnd	BS		WS		BPnd		SBR 60–90 min	
	Mean	SD	Mean	SD		SD	%CV	SD	%CV	%VAR ± SD	ICC	%VAR ± SD	ICC
Putamen_r	15.50 ± 3.78		15.47 ± 2.59		15.48	3.06	19.73	0.71	4.10	5.80 ± 4.79	0.91	6.90 ± 5.14	0.94
Putamen_t_ant	13.46 ± 1.48		14.08 ± 2.94		14.91	3.13	20.98	0.65	3.89	5.49 ± 3.02	0.95	6.40 ± 4.96	0.95
Putamen_r_post	14.03 ± 0.83		14.39 ± 2.08		15.20	3.18	20.94	1.13	6.65	9.41 ± 5.89	0.80	8.20 ± 5.02	0.90
Putamen_l	13.85 ± 1.01		14.40 ± 2.94		15.08	2.98	19.77	0.50	2.93	4.14 ± 3.20	0.96	7.41 ± 4.30	0.94
Putamen_l_ant	13.50 ± 1.12		14.11 ± 3.03		14.84	2.99	20.17	0.66	4.18	5.92 ± 2.29	0.95	7.40 ± 4.14	0.94
Putamen_l_post	14.25 ± 0.96		14.77 ± 2.87		15.38	3.03	19.69	0.86	5.41	7.65 ± 3.16	0.93	8.38 ± 5.11	0.92
CaudateNucl_l	11.00 ± 0.57		11.25 ± 2.81		12.32	2.55	20.68	0.57	4.21	5.96 ± 4.54	0.95	8.80 ± 4.54	0.94
CaudateNucl_r	10.93 ± 0.63		10.96 ± 2.60		11.99	2.38	19.82	0.51	4.36	6.17 ± 4.96	0.95	9.70 ± 5.07	0.90
NuclAccumb_l	9.86 ± 1.35		10.48 ± 1.91		10.73	1.84	17.17	0.48	4.53	6.40 ± 4.08	0.93	11.14 ± 5.03	0.89
NuclAccumb_r	10.76 ± 1.42		11.48 ± 2.75		11.55	2.65	22.92	0.55	4.45	6.30 ± 4.18	0.95	12.99 ± 8.32	0.60
SNpc_l	3.51 ± 0.24		3.54 ± 0.17		3.55	0.16	4.44	0.12	3.26	4.61 ± 2.16	0.47	2.63 ± 1.36	0.98
SNpc_r	3.44 ± 0.39		3.59 ± 0.32		3.61	0.37	10.18	0.14	3.71	5.24 ± 3.36	0.79	7.06 ± 7.50	0.83
Putamen	13.76 ± 1.07		14.29 ± 2.74		15.04	3.03	20.11	0.61	3.52	4.97 ± 3.85	0.94	7.15 ± 4.71	0.94
Putamen_ant	13.48 ± 1.30		14.09 ± 2.95		14.87	3.06	20.56	0.56	3.36	4.76 ± 3.63	0.96	6.87 ± 4.37	0.95
Putamen_post	14.16 ± 0.88		14.58 ± 2.47		15.29	3.09	20.20	0.99	6.01	8.50 ± 3.52	0.88	8.29 ± 5.03	0.91
CaudateNucl	10.96 ± 0.59		11.10 ± 2.64		12.15	2.45	20.16	0.51	4.08	5.77 ± 3.69	0.96	9.57 ± 4.98	0.92
NuclAccumb	10.27 ± 1.40		10.93 ± 2.18		10.97	1.91	17.44	0.48	4.37	6.18 ± 3.16	0.95	11.86 ± 3.30	0.82
SN_{pc}	3.46 ± 0.33		3.54 ± 0.22		3.57	0.26	7.23	0.11	3.01	4.26 ± 1.77	0.80	4.75 ± 3.71	0.93

duration and found the same relationship as for BP_{nd} values but slightly shorter imaging windows with SBRs at equilibrium (see Fig. 4). Nevertheless, both static frames from 60 to 90 and 75 to 90 min p.i. are within 95% of peak SBR, show excellent correlation with PB_{nd} values although overestimating BP_{nd} values about 50%. This time window is markedly shorter than the incubation time required for DATscan™ imaging (3–6 h), which bodes well for patient management [26].

The observed variability of BP_{nd} values was very good in all brain regions and ICC values were poor for left SNpc but very good for all other regions. In general, poor reliability might also relate to a small number of subjects or repetitions [27]. $n = 5$ HCs included in this test-retest study still represent a relatively small number of subjects and reliability in some regions might be low for statistical effects. Since right and total SNpc show good reliability, this is not really an issue at this point and we would expect that, at larger group sizes, the quantification outcome would be reliable in all regions. For SBRs derived from static scans, VAR is slightly higher than for dynamic quantification but still acceptable and reliability of static image quantification is very good in high-density DAT regions.

Overall, our data strongly indicate that [^{18}F]PR04.MZ is an excellent PET tracer for imaging and quantification of DAT in the human brain.

Conclusion

[^{18}F]PR04.MZ is a highly selective PET tracer for imaging of DAT in the human brain, providing good brain uptake, excellent imaging contrast, and stable, reliable quantification outcomes within a reasonable time frame. [^{18}F]PR04.MZ is metabolized quickly and no lipophilic, BBB-penetrating metabolites were observed. Both invasive 2TCM and SRTM are suitable for quantification via kinetic modeling and stable measurement outcomes can be obtained between 90 and until 130 min p.i. in all regions. Using a static imaging protocol, average SBR values between 60 and 90 min p.i. provide good estimates of BP_{nd} for quantification. Test-retest variability is low and provides excellent reliability of BP_{nd} values in repeated scans. The high specific uptake in SNpc is an advantage over existing methods and may have a clinical impact for patients being evaluated for movement disorders [19, 28]. The straightforward quantification of DAT availability using PR04.MZ in combination with the static imaging protocol validated herein bodes well for potential routine clinical application of the tracer for DAT-PET imaging. In summary, we believe that our results prove the clinical potential of this new tracer and support further studies in different indications.

Acknowledgments We would like to thank Dr. Geoff Warnock (PMod Technologies), Irene Coudeu, and Ana Hurtado (Positronmed) for their help during PET studies; Dr. Evelyng Faure (FALP, Chile) for acquiring MRI scans and Carlos Elgueta; and Dr. Mario Avila (Positronpharma) for assistance in tracer production.

Funding information This study was in part funded by the InnovaChile (CORFO), project 13PIE-21682. Carlos Juri was funded by Conicyt-Chile, project FONDECYT 11130534.

Compliance with ethical standards All procedures performed in studies involving human participants were in accordance with the ethical standards of the institutional and national research committee and with the principles of the 1964 Declaration of Helsinki and its later amendments or comparable ethical standards. The study was approved by the regional ethics committee board (CEC SSM Oriente, permit 20140520) and written informed consent has been obtained from all participants.

Conflict of interest The authors declare that they have no conflict of interest.

References

1. Vaughan RA, Foster JD. Mechanisms of dopamine transporter regulation in normal and disease states. Trends Pharmacol Sci. 2013;34(9):489–96.
2. Bannon MJ. The dopamine transporter: role in neurotoxicity and human disease. Toxicol Appl Pharmacol. 2005;204(3):355–60.
3. Strafella AP, Bohnen NI, Perlmutter JS, et al. Molecular imaging to track Parkinson's disease and atypical parkinsonisms: New imaging frontiers. Mov Disord. 2017;32(2):181–92.
4. Dickson DW, Braak H, Duda JE, et al. Neuropathological assessment of Parkinson's disease: refining the diagnostic criteria. Lancet Neurol. 2009;8(12):1150–7.
5. Yaqub M, Boellaard R, van Berckel BN, et al. Quantification of dopamine transporter binding using [^{18}F]FP-beta-CIT and positron emission tomography. J Cereb Blood Flow Metab. 2007;27(7):1397–406.
6. Sasaki T, Ito H, Kimura Y, et al. Quantification of dopamine transporter in human brain using PET with ^{18}F-FE-PE2I. J Nucl Med. 2012;53(7):1065–73.
7. Nye JA, Votaw JR, Bremmer JD, et al. Quantification of dopamine transporter density with [^{18}F]FECNT PET in healthy humans. Nucl Med Biol. 2014;41(3):217–22.
8. Kazumata K, Dhawan V, Chaly T, et al. Dopamine transporter imaging with fluorine-18-FPCIT and PET. J Nucl Med. 1998;39(9):1521–30.
9. Ariclot N, Vercouillie J, Malherbe C, et al. PET imaging of dopamine transporter with ^{18}F-LBT999: first human exploration. J Nucl Med. 2017;58(suppl 1):276.
10. Lee I, Kim JS, Park JY, et al. Head-to-head comparison of ^{18}F-FP-CIT and ^{123}I-FP-CIT for dopamine transporter imaging in patients with Parkinson's disease: a preliminary study. Synapse. 2018;72(7):e22032.
11. Jakobson Mo S, Axelsson J, Jonasson L, et al. Dopamine transporter imaging with [^{18}F]FE-PE2I PET and [^{123}I]FP-CIT SPECT-a clinical comparison. EJNMMI Res. 2018;8(1):100.
12. Riss PJ, Hummerich R, Schloss P. Synthesis and monoamine uptake inhibition of conformationally constrained 2beta-carbomethoxy-3beta-phenyl tropanes. Org Biomol Chem. 2009;7(13):2688–98.

13. Riss PJ, Debus F, Hummerich R, et al. Ex vivo and in vivo evaluation of [^{18}F]PR04.MZ in rodents: a selective dopamine transporter imaging agent. ChemMedChem. 2009;4(9):1480–7.
14. Goodman MM, Kilts CD, Keil R, et al. ^{18}F-labeled FECNT: a selective radioligand for PET imaging of brain dopamine transporters. Nucl Med Biol. 2000;27(1):1–12.
15. Chalon S, Hall H, Saba W, et al. Pharmacological characterization of (E)-N-(4-fluorobut-2-enyl)-2beta-carbomethoxy-3beta-(4′-tolyl)nortropane (LBT-999) as a highly promising fluorinated ligand for the dopamine transporter. J Pharmacol Exp Ther. 2006;317(1):147–52.
16. Chalon S, Garreau L, Emond P, et al. Pharmacological characterization of (E)-N-(3-iodoprop-2-enyl)-2beta-carbomethoxy-3beta-(4′-methylphenyl)n ortropane as a selective and potent inhibitor of the neuronal dopamine transporter. J Pharmacol Exp Ther. 1999;291(2):648–54.
17. Riss PJ, Roesch F. Efficient microwave-assisted direct radiosynthesis of [^{18}F]PR04.MZ and [^{18}F]LBT999: selective dopamine transporter ligands for quantitative molecular imaging by means of PET. Bioorg Med Chem. 2009;17(22):7630–4.
18. Riss PJ, Hooker JM, Shea C, et al. Characterisation of [^{11}C]PR04.MZ in Papio anubis baboon: a selective high-affinity radioligand for quantitative imaging of the dopamine transporter. Bioorg Med Chem Lett. 2012;22(1):679–82.
19. Juri C, Chana P, Kramer V, et al. Imaging nigrostriatal dopaminergic deficit in Holmes tremor with ^{18}F-PR04.MZ-PET/CT. Clin Nucl Med. 2015;40(9):740–1.
20. Kramer V, Juri C, Chana-Cuevas P, et al. Dopamine transporter quantification by PET with [^{18}F]PR04.MZ in patients with early Parkinson's disease. J Nucl Med. 2014;55(suppl 1):1829.
21. Kramer V, Pruzzo R, Chana-Cuevas P, et al. Initial human PET studies with [^{18}F]PR04.MZ for quantification of striatal and extrastriatal dopamine transporters. J Nucl Med. 2013;54(suppl 2):416.
22. Hammers A, Allom R, Koepp MJ, et al. Three-dimensional maximum probability atlas of the human brain, with particular reference to the temporal lobe. Hum Brain Mapp. 2003;19(4):224–47.
23. Lammertsma AA, Bench CJ, Hume SP, et al. Comparison of methods for analysis of clinical [^{11}C]raclopride studies. J Cereb Blood Flow Metab. 1996;16:10.
24. Lammertsma AA, Hume SP. Simplified reference tissue model for PET receptor studies. NeuroImage. 1996;4(3):153–8.
25. Baumgartner R, Joshi A, Feng D, Zanderigo F, Ogden RT. Statistical evaluation of test-retest studies in PET brain imaging. EJNMMI Res. 2018;8(1):13.
26. Darcourt J, Booij J, Tatsch K et al. EANM procedure guidelines for brain neurotransmission SPECT using (123)I-labelled dopamine transporter ligands, version 2. Eur J Nucl Med Mol Imaging. 2010;37(2):443–50.
27. Koo TK, Li MY. A guideline of selecting and reporting intraclass correlation coefficients for reliability research. J Chiropr Med. 2016;15(2):155–63.
28. Chana-Cuevas P, Juri C, Kramer V et al. 2016 Quantification of striatal dopamine transporters with [^{18}F]PR04.MZ in patients with progressive supranuclear palsy and Parkinson's disease. Mov Disord.;31(suppl 2). https://www.mdsabstracts.org/abstract/quantification-of-striatal-dopamine-transporters-with-18fpr04-mz-in-patients-with-progressive-supranuclear-palsy-and-parkinsons-disease/.

Key points

Question: To study and describe the pharmacokinetics and an adequate imaging and quantification protocol for [^{18}F]PR04.MZ.

Pertinent findings: We evaluated metabolism, regional brain uptake, kinetic modeling, impact of scan duration, and test-retest variability and showed that [^{18}F]PR04.MZ is a highly selective PET tracer for DAT, providing excellent imaging contrast and stable, reliable quantification outcomes within a reasonable time frame.

Implications for patient care: The high specific uptake, in particular, in SNpc is an advantage over existing methods and may have a clinical impact for patients being evaluated for movement disorders.

Affiliations

Vasko Kramer[1,2] · Carlos Juri[3,4] · Patrick J. Riss[5] · Rossana Pruzzo[1] · Cristian Soza-Ried[1] · Jonathan Flores[1] · Ana Hurtado[1] · Frank Rösch[6] · Pedro Chana-Cuevas[7,8] · Horacio Amaral[1,2]

1 Center for Nuclear Medicine & PET/CT Positronmed, Julio Prado 714, Santiago, Chile

2 Positronpharma SA, Santiago, Chile

3 Department of Neurology, Faculty of Medicine, Pontificia Universidad Católica de Chile, Santiago, Chile

4 Department of Neurology, Hospital Sotero del Río, Santiago, Chile

5 Department of Chemistry, University of Oslo, Oslo, Norway

6 Institute of Nuclear Chemistry, Johannes Gutenberg-University, Mainz, Germany

7 Centro de Trastornos del Movimiento, Santiago, Chile

8 Facultad de Ciencias Médicas, Universidad de Santiago de Chile, Santiago, Chile